

Meson Spectroscopy at COMPASS

Boris Grube¹ on behalf of the COMPASS collaboration

¹ Physik-Department E18, Technische Universität München, Garching, Germany

E-mail: bgrube@tum.de

Abstract. The COmmon Muon and Proton Apparatus for Structure and Spectroscopy (COMPASS) is a multi-purpose fixed-target experiment at the CERN Super Proton Synchrotron (SPS) aimed at studying the structure and spectrum of hadrons. The two-stage spectrometer has a good acceptance for charged as well as neutral particles over a wide kinematic range and thus allows to access a wide range of reactions. Light mesons are studied with negative (mostly π^-) and positive (p , π^+) hadron beams with a momentum of 190 GeV/c. The spectrum of light mesons is investigated in various final states produced in diffractive dissociation reactions at squared four-momentum transfers to the target between 0.1 and 1.0 (GeV/c)². The flagship channel is the $\pi^-\pi^+\pi^-$ final state, for which COMPASS has recorded the currently largest data sample. These data not only allow to measure the properties of known resonances with high precision, but also to search for new states. Among these is a new resonance-like signal, the $a_1(1420)$, with unusual properties. Of particular interest is also the resonance content of the partial wave with spin-exotic $J^{PC} = 1^{-+}$ quantum numbers, which are forbidden for quark-antiquark states.

1. Introduction

The COMPASS experiment has recorded a large data set of the diffractive dissociation reaction $\pi^- + p \rightarrow (3\pi)^- + p_{\text{recoil}}$ using a 190 GeV/c pion beam on a liquid-hydrogen target. This reaction is known to exhibit a rich spectrum of produced intermediate three-pion states. In the past, several candidates for spin-exotic mesons have been reported in pion-induced diffraction [1]. In diffractive reactions the beam hadron is excited to some intermediate state X^- via t -channel Reggeon exchange with the target. At 190 GeV/c beam momentum, pomeron exchange is dominant. In the reaction considered here, the X decays into the $\pi^-\pi^+\pi^-$ and $\pi^-\pi^0\pi^0$ final states, which are detected by the spectrometer. The scattering process is characterized by two kinematic variables: the squared total center-of-mass energy s and the squared four-momentum transfer to the target $t = (p_{\text{beam}} - p_X)^2 < 0$. It is customary to use the reduced four-momentum transfer $t' \equiv |t| - |t|_{\text{min}}$ instead of t , where $|t|_{\text{min}}$ is the minimum value of $|t|$ for a given invariant mass of X . After all cuts, the data sample consists of 46×10^6 $\pi^-\pi^+\pi^-$ and 3.5×10^6 $\pi^-\pi^0\pi^0$ exclusive events in the analyzed kinematic region of three-pion mass, $0.5 < m_{3\pi} < 2.5$ GeV/c², and four-momentum transfer squared, $0.1 < t' < 1.0$ (GeV/c)². Figure 1 shows the $\pi^-\pi^+\pi^-$ mass spectrum as well as that of the $\pi^+\pi^-$ subsystem. The known pattern of resonances $a_1(1260)$, $a_2(1320)$, and $\pi_2(1670)$ is seen in the 3π system along with $\rho(770)$, $f_0(980)$, $f_2(1270)$, and $\rho_3(1690)$ in the $\pi^+\pi^-$ subsystem.

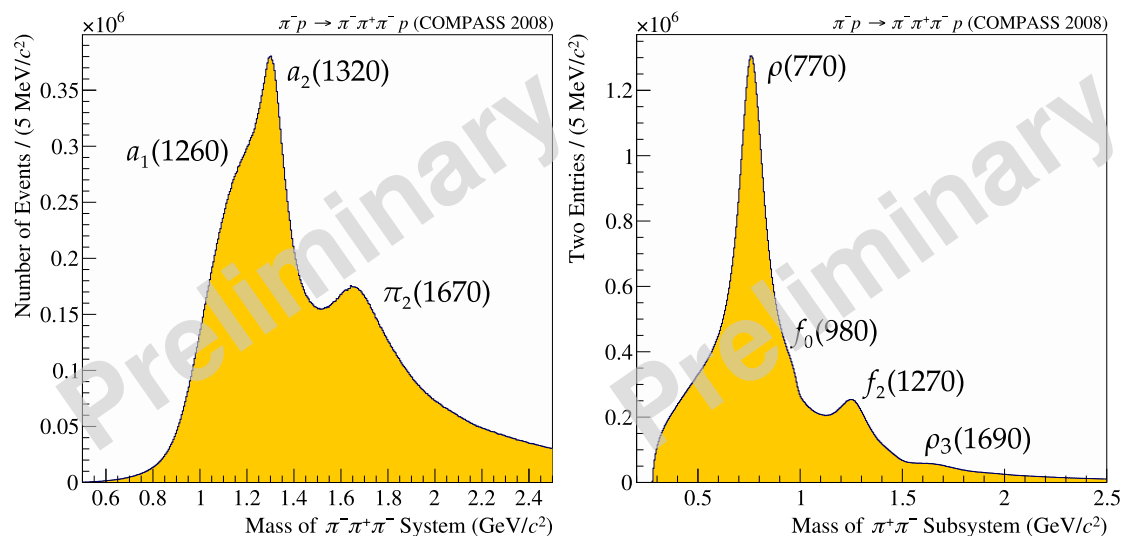


Figure 1. Left: $\pi^- \pi^+ \pi^-$ invariant mass spectrum in the analyzed range; Right: $\pi^+ \pi^-$ mass distribution.

2. Partial-Wave Decomposition

In order to disentangle the different contributing intermediate 3π states X , a partial-wave analysis (PWA) was performed. The PWA is based on the isobar model, which assumes that the X decays first into an intermediate resonance, which is called the isobar, and a “bachelor pion”. In a second step, the isobar decays into $\pi^+ \pi^-$. In accordance with the $\pi^+ \pi^-$ invariant mass spectrum shown in Fig. 1 and with analyses by previous experiments, we include $[\pi\pi]_S$, $\rho(770)$, $f_0(980)$, $f_2(1270)$, $f_0(1500)$, and $\rho_3(1690)$ as isobars into the fit model. Here, $[\pi\pi]_S$ represents the broad component of the $\pi\pi$ S -wave. Based on the six isobars, we have constructed a set of partial waves that consists of 88 waves in total, including one non-interfering flat wave representing three uncorrelated pions. This constitutes the largest wave set ever used in an analysis of the 3π final state. The partial-wave decomposition is performed in narrow bins of the 3π invariant mass and makes no assumptions on the 3π resonance content of the partial waves. Each $m_{3\pi}$ bin is further subdivided into non-equidistant bins in the four-momentum transfer t' . For the $\pi^- \pi^+ \pi^-$ channel 11 bins are used, for the $\pi^- \pi^0 \pi^0$ final state 8 bins. With this additional binning in t' , the dependence of the partial-wave amplitudes on the four-momentum transfer can be studied in detail. The details of the analysis model are described in Ref. [2].

The partial-wave amplitudes are extracted from the data as a function of $m_{3\pi}$ and t' by fitting the five-dimensional kinematic distributions of the outgoing three pions. The amplitudes do not only contain information about the partial-wave intensities, but also about the relative phases of the partial waves. The latter are crucial for resonance extraction.

Partial waves are defined by the quantum numbers of the X (spin J , parity P , C -parity, spin projection M), the naturality $\epsilon = \pm 1$ of the exchange particle, the isobar, and the orbital angular momentum L between the isobar and the bachelor pion. These quantities are summarized in the partial-wave notation $J^{PC} M^\epsilon [\text{isobar}] \pi L$. Since at the used beam energies pomeron exchange is dominant, 80 of the 88 partial waves in the model have $\epsilon = +1$. The C -parity is by convention that of the neutral isospin partner of the X^- .

3. The $J^{PC} = 1^{-+}$ Spin-Exotic Wave

The 88-wave model contains also spin-exotic waves with J^{PC} quantum numbers that are forbidden for quark-antiquark states in the non-relativistic limit. The most interesting of these

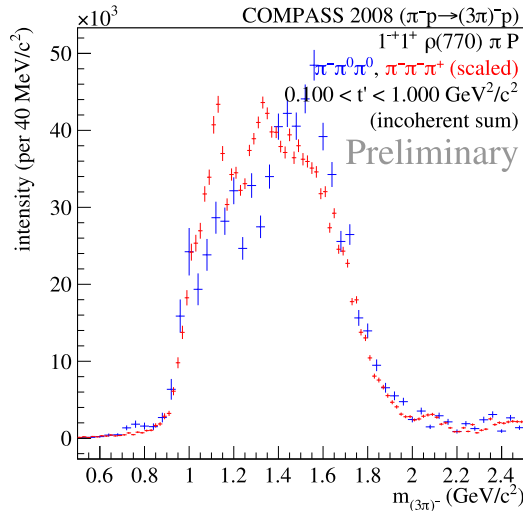


Figure 2. Intensity of the $1^{-+} 1^{+} \rho(770) \pi P$ wave summed over all t' bins for the $\pi^{-} \pi^{+} \pi^{-}$ (red) and the $\pi^{-} \pi^{0} \pi^{0}$ (blue) final state.

waves is the $1^{-+} 1^{+} \rho(770) \pi P$ wave, which contributes less than 1% to the total intensity. Previous analyses claimed a resonance, the $\pi_1(1600)$, at about $1.6 \text{ GeV}/c^2$ in this channel [3, 4]. Figure 2 shows the intensity of this partial wave for the two final states ($\pi^{-} \pi^{+} \pi^{-}$ in red, $\pi^{-} \pi^{0} \pi^{0}$ in blue). The two distributions are scaled to have the same integral.

Both decay channels are in fair agreement and exhibit a broad enhancement extending from about 1.0 to $1.8 \text{ GeV}/c^2$. In the 1.0 to $1.2 \text{ GeV}/c^2$ mass range the intensity depends strongly on the details of the fit model. Peak-like structures in this region are probably due to imperfections of the applied PWA model. A remarkable change of the shape of the intensity spectrum of the $1^{-+} 1^{+} \rho(770) \pi P$ wave with t' is observed (see Fig. 3). At values of t' below about $0.3 (\text{GeV}/c)^2$, we observe no indication of a resonance peak around $m_{3\pi} = 1.6 \text{ GeV}/c^2$, where we would expect the $\pi_1(1600)$. For the t' bins in the interval from 0.449 to $1.000 (\text{GeV}/c)^2$, the observed intensities exhibit a very different shape as compared to the low- t' region, with a structure emerging at about $1.6 \text{ GeV}/c^2$ and the intensity at lower masses disappearing rapidly with increasing t' . This is in contrast to clean resonance signals like the $a_2(1320)$ in the $2^{++} 1^{+} \rho(770) \pi D$ wave, which, as expected, do not change their shape with t' (see Fig. 4). The observed t' behavior of the 1^{-+} wave is therefore a strong indication that non-resonant contributions play a dominant role.

It is believed that the non-resonant contribution in the 1^{-+} wave originates predominantly from the Deck effect, in which the incoming beam pion dissociates into the isobar and an off-shell pion that scatters off the target proton to become on-shell [5]. As a first step towards a better understanding of the non-resonant contribution, Monte-Carlo data were generated that are distributed according to a model of the Deck effect. The model employed here is very similar to that used in Ref. [6]. The partial-wave projection of these Monte Carlo data is shown as green points in Fig. 3. In order to compare the intensities of real data and the Deck-model pseudo data, the Monte Carlo data are scaled to the t' -summed intensity of the 1^{-+} wave as observed in real data. At values of t' below about $0.3 (\text{GeV}/c)^2$, the intensity distributions of real data and Deck Monte Carlo exhibit strong similarities suggesting that the observed intensity might be saturated by the Deck effect. Starting from $t' \approx 0.4 (\text{GeV}/c)^2$, the spectral shapes for Deck pseudo-data and real data deviate from each other with the differences increasing towards larger values of t' . This leaves room for a potential resonance signal. It should be noted, however, that

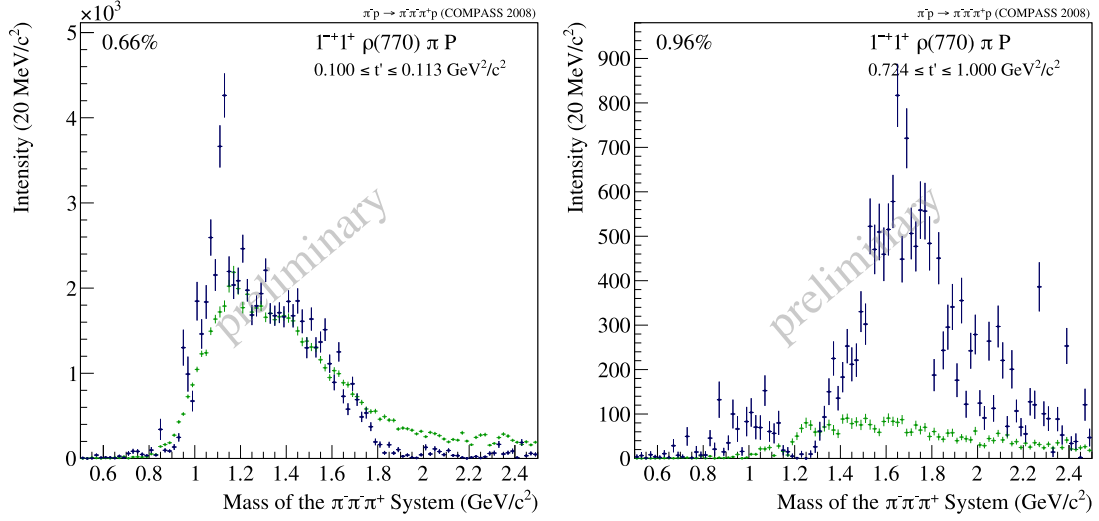


Figure 3. Intensity of the $1^{-+} 1^{+} \rho(770) \pi P$ wave in different regions of t' for the $\pi^{-} \pi^{+} \pi^{-}$ final state (dark blue). The partial-wave projections of Monte-Carlo data generated according to a model of the Deck effect are overlaid in green.

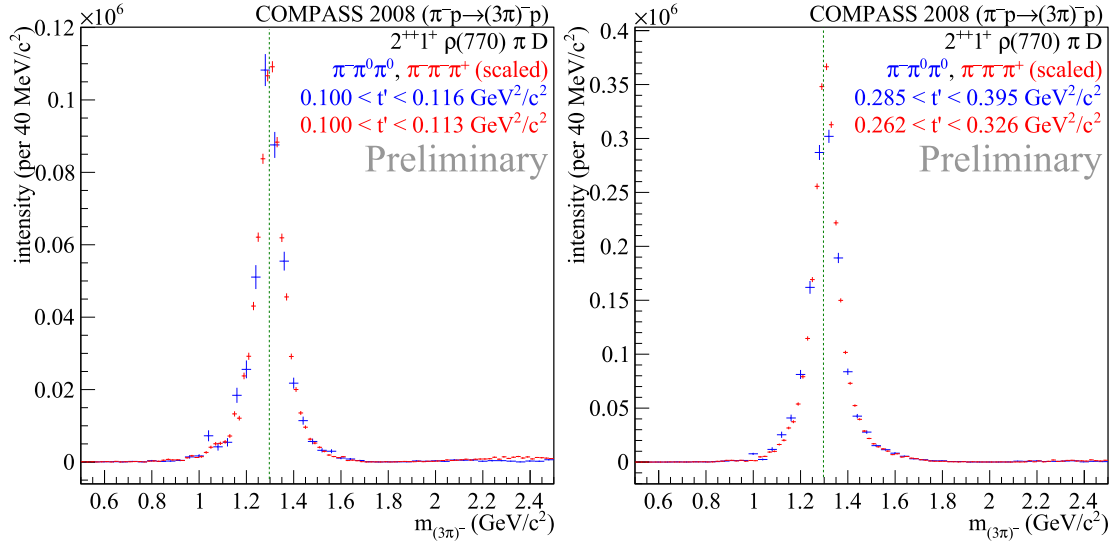


Figure 4. Intensity of the $2^{++} 1^{+} \rho(770) \pi D$ wave in different regions of t' for the $\pi^{-} \pi^{+} \pi^{-}$ (red) and the $\pi^{-} \pi^0 \pi^0$ (blue) final state.

the Deck pseudo data contain no resonant contributions. Therefore, potential interference effects between the resonant and non-resonant amplitudes cannot be assessed in this simple approach.

4. The $a_1(1420)$

A surprising find in the COMPASS data was a pronounced narrow peak at about $1.4 \text{ GeV}/c^2$ in the $1^{++} 0^{+} f_0(980) \pi P$ wave (see Fig. 5). The peak is observed with similar shape in the $\pi^{-} \pi^{+} \pi^{-}$ and $\pi^{-} \pi^0 \pi^0$ data and is robust against variations of the PWA model. In addition to the peak in the partial-wave intensity, rapid phase variations with respect to most waves are observed in the $1.4 \text{ GeV}/c^2$ region (see Fig. 6). The phase motion as well as the peak shape

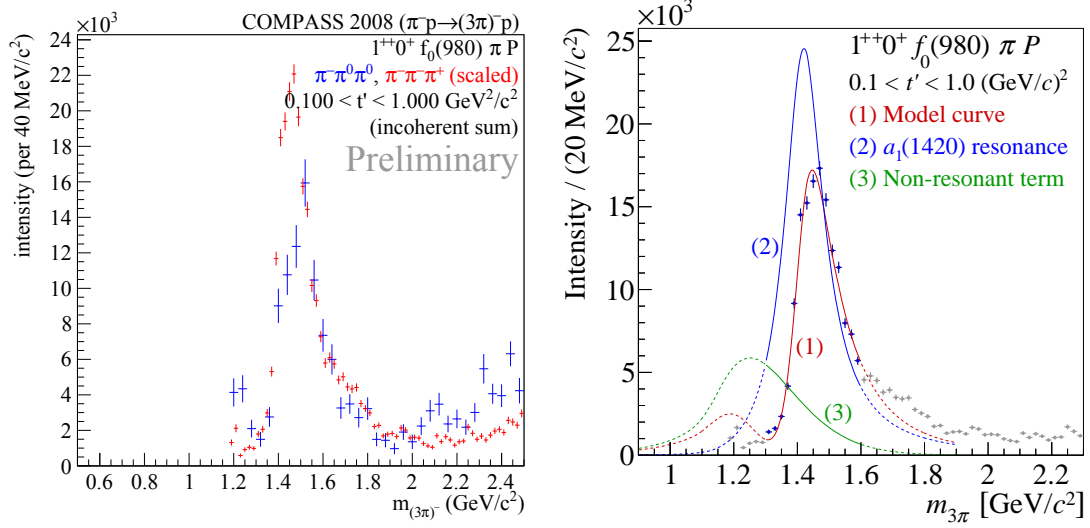


Figure 5. Left: Intensity of the $1^{++} 0^+ f_0(980) \pi P$ wave summed over all t' bins for the $\pi^- \pi^+ \pi^-$ (red) and the $\pi^- \pi^0 \pi^0$ (blue) final states. Right: Result of a resonance-model fit to the $\pi^- \pi^+ \pi^-$ data [7]. The data points correspond to the red points in the left figure.

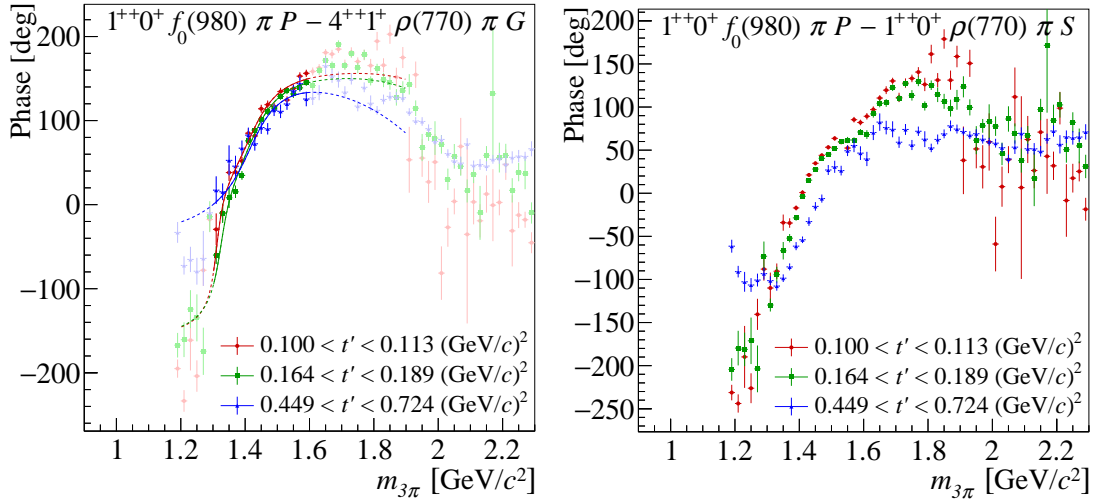


Figure 6. Examples for relative phases of the $1^{++} 0^+ f_0(980) \pi P$ wave with respect to the $4^{++} 1^+ \rho(770) \pi G$ (left) and the $1^{++} 0^+ \rho(770) \pi S$ wave (right) [7]. The phases are shown for three different t' regions indicated by the color.

change only little with t' .

In order to test the compatibility of the signal with a Breit-Wigner resonance, a resonance-model fit was performed using a novel method, where the intensities and relative phases of three waves ($1^{++} 0^+ f_0(980) \pi P$, $2^{++} 1^+ \rho(770) \pi D$, and $4^{++} 1^+ \rho(770) \pi G$) were fit simultaneously in all 11 t' bins [7]. Forcing the resonance parameters to be the same across all t' bins leads to an improved separation of resonant and non-resonant contribution as compared to previous analyses that did not incorporate the t' information. The Breit-Wigner model describes the peak in the $1^{++} 0^+ f_0(980) \pi P$ wave well and yields a mass of $m_0 = 1414_{-13}^{+15}$ MeV/c² and a width of $\Gamma_0 = (153_{-23}^{+8})$ MeV/c² for the $a_1(1420)$. Due to the high precision of the data, the

uncertainties are dominated by systematic effects.

The $a_1(1420)$ signal is remarkable in many ways. It appears in a mass region that is well studied since decades. However, previous experiments were unable to see the peak, because it contributes only 0.25% to the total intensity. The $a_1(1420)$ is very close in mass to the 1^{++} ground state, the $a_1(1260)$. But it has a much smaller width than the $a_1(1260)$. The $a_1(1420)$ peak is seen only in the $f_0(980)\pi$ decay mode of the 1^{++} waves and lies suspiciously close to the $K\bar{K}^*(892)$ threshold.

The nature of the $a_1(1420)$ is still unclear and several interpretations were proposed. It could be the isospin partner to the $f_1(1420)$. It was also described as a two-quark-tetraquark mixed state [8] and a tetraquark with mixed flavor symmetry [9]. Other models do not require an additional resonance: Ref. [10, 11] proposes resonant re-scattering corrections in the Deck process as an explanation, whereas Ref. [12] suggests a branching point in the triangle rescattering diagram for $a_1(1260) \rightarrow K\bar{K}^*(892) \rightarrow K\bar{K}\pi \rightarrow f_0(980)\pi$. More detailed studies are needed in order to distinguish between these models.

Acknowledgments

This work was supported by the BMBF, the MLL and the Cluster of Excellence Exc153 “Origin and Structure of the Universe”.

References

- [1] C. Meyer et al., *Phys. Rev. C* **82** (2010) 025208; E. Klempt et al., *Phys. Rept.* **454** (2007) 1.
- [2] C. Adolph et al. (COMPASS Collaboration), arXiv:1509.00992 (2015), submitted to *Phys. Rev. D*.
- [3] S. Chung et al. (E852 Collaboration), *Phys. Rev. D* **60** (1999) 092001.
- [4] M. Alekseev et al. (COMPASS Collaboration), *Phys. Rev. Lett.* **104** (2010) 241803.
- [5] R. T. Deck, *Phys. Rev. Lett.* **13** (1964) 169.
- [6] C. Daum et al. (ACCMOR Collaboration), *Nucl. Phys. B* **182** (1981) 269.
- [7] C. Adolph et al. (COMPASS Collaboration), *Phys. Rev. Lett.* **115** (2015) 082001.
- [8] Z.-G. Wang, arXiv:1401.1134 (2014).
- [9] H.-X. Chen et al., *Phys. Rev. D* **91** (2015) 094022.
- [10] J.-L. Basdevant and E. L. Berger, *Phys. Rev. Lett.* **114** (2015) 192001.
- [11] J.-L. Basdevant and E. L. Berger, arXiv:1501.04643 (2015).
- [12] M. Mikhasenko et al., *Phys. Rev. D* **91** (2015) 094015.